Protein−Protein Interactions Dominate the Assembly Thermodynamics of a Transcription Repression Complex†

Huaying Zhao, Emily Streaker, Weilan Pan,‡ and Dorothy Beckett*

Department of Chemistry & Biochemistry, College of Chemical & Life Sciences, Center for Biological Structure & Organization, University of Maryland, College Park, Maryland 20742

Received July 3, 2007; Revised Manuscript Received August 29, 2007

ABSTRACT: Assembly of the transcription repression complex at the *Escherichia coli* biotin biosynthetic operon occurs via coupled protein−protein and protein−DNA interactions in which the holoBirA dimer binds to the forty base pair biotin operator sequence. The thermodynamic driving forces for the assembly process have been dissected using sedimentation equilibrium measurements and DNaseI footprint titrations. Measurements of the temperature dependence of dimerization indicate that this process is strongly enthalpically opposed and is driven by a very favorable entropy. By contrast, the DNA binding step is enthalpically driven and opposed by a modest entropy. Neither step is accompanied by a heat capacity change. The convoluted protein−protein and protein−DNA binding reaction is dominated by the thermodynamic signature of the dimerization step. This observed dominance of the dimerization step illustrates the importance of dissecting complex DNA binding reactions into their constituent steps in elucidation of the thermodynamic driving forces for these processes. Measurements of the salt dependence of dimerization and DNA binding indicate modest contributions of electrostatic interactions to each contributing step as well as the total assembly of the repression complex. In light of the known structural features of this system, this modest dependence of the DNA binding equilibrium on salt concentration was unanticipated.

Initiation of the genome-based processes including transcription, replication, or repair requires assembly of protein complexes at specific sites on the genomic DNA. In transcription regulation the occupancy of a DNA site by the appropriate regulatory protein dictates the level of expression of a gene or operon. Since occupancy is determined by, among other factors, the assembly energetics of the relevant protein−DNA complex, a molecular understanding of transcription regulation requires measurement of the energetics and determination of the driving forces for the assembly. Biochemical and structural characterization of transcriptional regulatory proteins reveals that many form oligomers. Thus, in considering the assembly energetics, both protein−protein and protein−DNA interactions must be accounted for. Some transcriptional regulatory proteins, such as the purine, tryptophan, and lactose repressors, form stable oligomers that undergo no change in assembly state in the course of DNA binding (*1*−*7*). Others, including the bacteriophage *λ c*I and cro repressors, bind to DNA in a mechanism involving coupled self-association (*8*, *9*). For these latter proteins, determining the energetics of regulatory complex assembly requires measurement of both steps in the process. In assembly of eukaryotic transcriptional regulatory proteins on DNA the energetics and specificity of the protein−protein interactions can play important roles in dictating the transcriptional outcome. For example, in the mammalian basic helix−loop−helix/PAS family of transcriptional regulators the choice of dimerization partner determines the target gene at which regulation occurs (*10*).

In systems characterized by coupled protein−protein and protein−DNA interactions that have been subjected to rigorous thermodynamic analysis the protein assembly step can contribute significantly to the total assembly energetics. For example, in binding of the bacteriophage *λ c*I repressor to the right operator site O_R1, the Gibbs free energy of protein assembly is −11 kcal/mol (*11*) and binding of the dimer to DNA (O_R1) is −12 kcal/mol(*12*). By contrast, dimerization of bacteriophage *λ* cro protein occurs with a modest Gibbs free energy of −8.7 kcal/mol while binding to the right operator site O_R3 occurs with a free energy of −12.5 kcal/mol (*9*). The physical-chemical forces that drive DNA binding by transcriptional regulatory proteins can vary over a broad range (*13*), and dissection of the Gibbs free energy reveals that, while some are driven by large negative enthalpies and entropically opposed, others are entropically driven and opposed by large positive enthalpies. In some cases binding is accompanied by a large negative heat capacity change (*13*, *14*). Measurements of the salt dependence indicate that DNA binding is typically coupled to release of a number of cations from the DNA surface (*13*, *15*). Few systems that involve coupled protein assembly and DNA binding have been subjected to detailed thermodynamic analysis. Studies on the energetics of interactions between the *λ c*I repressor and the right operator region of bacteriophage *λ* showed that both repressor dimerization and dimer binding to DNA are enthalpically driven and that the enthalpy

† Supported by NIH Grants R01-GM46511 and S10-RR15899.

* Corresponding author. Phone: 301-405-1812. E-mail: dbeckett@umd.edu.

‡ Current address: E 353/327A, Experimental Station, DuPont Company, Wilmington, DE 19880.

10.1021/bi7013097 CCC: $37.00
Published on Web 11/01/2007

is nearly temperature-invariant (*12*, *16*). Moreover, while protein dimerization in the system is coupled to ion uptake, DNA binding is accompanied by a net ion release (*16*, *17*).

In the *Escherichia coli* biotin regulatory system, the BirA protein functions as a biotin protein ligase and as a transcriptional repressor (*18*, *19*). As the biotin ligase it performs the essential metabolic function of catalyzing biotin addition to the biotin-dependent carboxylase, acetyl-CoA carboxylase (ACC). As the repressor of transcription initiation at the biotin biosynthetic operon, BirA binds to the biotin operator, bioO, to block transcription initiation at the operon's two divergent promoters. Assembly of BirA on DNA is a multistep process involving coupled dimerization and DNA binding (*20*). BirA is an allosteric DNA binding protein that catalyzes synthesis of its corepressor, biotinyl-5′-AMP (bio-5′-AMP), from substrates biotin and ATP (*21*). Interestingly the corepressor serves a second function as the intermediate in biotin transfer to acetyl-CoA carboxylase (*22*). The corepressor drives assembly of BirA onto the biotin operator by promoting its homodimerization (*23*). Indeed, bio-5′-AMP binding influences the energetics of the dimerization step, but not dimer binding to bioO, in repression complex assembly (*24*). Kinetic studies have demonstrated that DNA binding by holoBirA occurs in a mechanism involving dimerization followed by binding of this preformed dimer to bioO (*25*).

No structure of the $(holoBirA)_2$·bioO complex is yet available. However, structures of apoBirA, BirA bound to biotin, and BirA in complex with the corepressor analogue biotinol-5′-AMP (btnOH-AMP) have been solved by X-ray crystallography (*26*−*28*). ApoBirA is composed of three domains (Figure 1A). The N-terminal winged helix−turn−helix DNA binding domain is connected *via* a linker to the central catalytic domain, which is characterized by an SH2-like fold (*29*). The C-terminal domain forms an SH3-like fold and functions in dimerization and biotin transfer to acetyl-CoA carboxylase (*28*, *30*). Structures of both ligand-bound repressors are homodimeric. However, since btnOH-AMP is a better functional mimic of the physiological corepressor, bio-5′-AMP (*31*), the complex in which BirA is bound to this small molecule is of greater biological relevance than that in which the protein is bound to the substrate biotin. Discussion of the dimer structure is, therefore, limited to the $(BirA{\cdot}btnOH\text{-}AMP)_2$ complex. The dimer interface is an extended β-sheet that forms by side-by-side antiparallel alignment of the central domains of each monomer (Figure 1A). Three loops, one of which also functions in biotin and adenylate binding, from each monomer also participate directly in the interface. In addition to these central domain contacts, the interface extends to the protein's C-terminal domain. The distance between the two DNA binding domains in the dimer is approximately 65 Å, which is appropriate for interaction with the comparatively long 40 base-pair biotin operator (bioO). The bioO sequence is an imperfect inverted palindrome that can be characterized as tripartite with two 12 base-pair termini interrupted by a 16 base-pair central core (Figure 1B). Combined chemical and enzymatic footprinting have been utilized to characterize the protein−DNA interface (*32*). Results of dimethyl sulfate probing revealed that the two DNA binding domains of BirA directly interact with the major and minor grooves in the terminal 12 base-pair segments of the operator site. Hydroxyl-radical probing of the interface reveals protection of the phosphodiester backbone on one face of the double helix. This protection occurs at backbone positions in both 12 base-pair termini as well as in the 16 base-pair central core. Results of DNaseI footprinting are consistent with protein-induced DNA distortion that is localized to the backside of each of the operator termini and the central oligo-A tract at the core of the operator site(*32*).

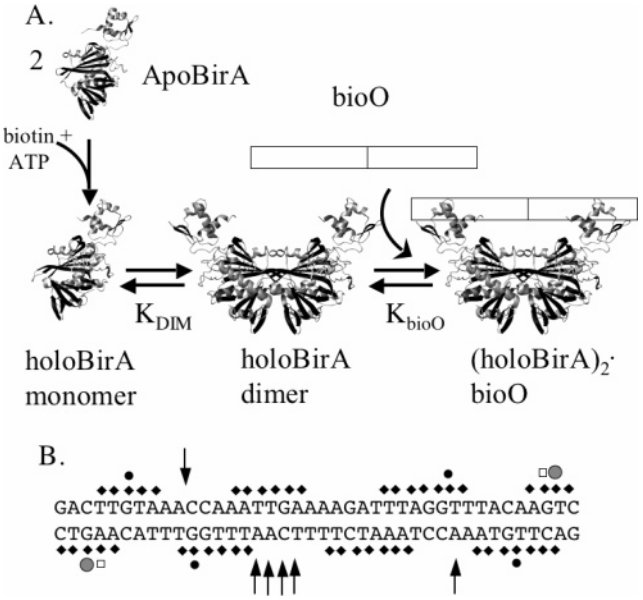

FIGURE 1: (A) Assembly of the $(holoBirA)_2$·bioO complex from apoBirA monomers and bioO DNA. BirA binds substrates biotin and ATP and catalyzes synthesis of the corepressor, bio-5′-AMP. The resulting holoBirA monomer dimerizes with an equilibrium association constant, K_{DIM}, and then binds to bioO with an equilibrium association constant, K_{bioO}. Protein structure models were created using MolMol (*42*) with 1BIA and 1BIB as input PDB files. The holoBirA monomer model was created by deleting one of the monomers from the holoBirA dimer model. (B) Sequence of the biotin operator with the results of solution structural probing highlighted. The diamonds represent sites of protection from hydroxyl radical-mediated cleavage. The filled circles represent sites of protection from (small circles) or enhancement of (large circles) dimethyl sulfate modification at guanine bases. The open squares represent sites of protection from dimethyl sulfate modification at adenine bases. The arrows represent sites of DNaseI hypersensitivity in the complex relative to the free DNA (*32*).

HoloBirA dimerization and total assembly of $(holoBirA)_2$·bioO have previously been subjected to limited thermodynamic analysis (*24*, *25*, *33*). The results indicate that in the standard buffer conditions utilized for these measurements (10 mM TrisHCl, pH 7.50 ± 0.02 at 20 °C, 200 mM KCl, 2.5 mM $MgCl_2$, 1.0 mM $CaCl_2$) the Gibbs free energy for total assembly is approximately −21 kcal/mol of which approximately −7 kcal/mol is attributed to dimerization and −14 kcal/mol to binding of the holoBirA dimer to bioO. Previous results also suggest a contribution of electrostatic interactions to protein assembly and DNA binding since both processes become less energetically favorable as the KCl concentration is increased from 50 mM to 200 mM(*24*).

In order to determine the driving forces associated with assembly of the $(holoBirA)_2$·bioO complex we have measured the temperature and salt dependence of the dimerization and total assembly. Sedimentation equilibrium measurements were employed to measure holoBirA self-association, and total assembly was measured using DNaseI footprint titra-

tions. Data analysis was used to deconvolute the dimerization from the DNA binding step in total assembly. Results of van't Hoff analysis of dimerization indicate that the process is enthalpically highly unfavorable and entropically highly favorable. By contrast, binding of the holoBirA dimer to bioO is enthalpically favorable and entropically moderately unfavorable. The thermodynamic signature of the dimerization process dominates the overall assembly thermodynamics. Measurements of the dependence of both dimerization and DNA binding on salt concentration indicate a modest net contribution of electrostatic interactions to each step in assembly of the $(holobirA)_2$·bioO complex.

MATERIALS AND METHODS

Chemicals and Biochemicals. The restriction endonucleases *Hin*dIII and *Pst*I and the Klenow fragment of DNA polymerase I were purchased from Promega. The α^{32}P dATP and dGTP used in radiolabeling of DNA were from GE Healthcare. The d-biotin, ATP, calf thymus DNA, tRNA, and DNaseI used in footprinting experiments were from Sigma-Aldrich. The corepressor, bio-5′-AMP, was synthesized as previously described (*20*, *22*). All other chemicals used in the preparation of buffers were reagent or analytical grade. The biotin repressor was purified as previously described (*31*).

Sedimentation Equilibrium Measurements. Sedimentation equilibrium was used to measure the assembly properties of holoBirA. Measurements were conducted using a Beckman Optima XL-I (Beckman-Coulter) analytical ultracentrifuge equipped with a four-hole An-60 rotor. Either 12 or 3 mm double-sectored cells with charcoal-filled Epon centerpieces and saffire windows were used. Sample volumes were 150 μL for the 12 mm cells and 50 μL for the 3 mm cells. Measurements of BirA dimerization made in the presence of bio-5′-AMP were performed under stoichiometric binding conditions with a bio-5′-AMP:BirA monomer molar ratio of 1.5:1. For all experiments apoBirA was first fully exchanged into the appropriate buffer using MicroBioSpin6 columns (BioRad). In experiments designed to measure the temperature-dependence of holoBirA dimerization the buffer was 10 mM Tris-HCl pH 7.50 (adjusted at the working temperature), 200 mM KCl, and 2.5 mM $MgCl_2$. For experiments in which the dependence of dimerization on salt concentration was measured the buffer composition was, with the exception of the KCl concentration, which ranged from 50 mM to 300 mM, 10 mM Tris-HCl pH 7.50 ± 0.02 at 20 °C, 2.5 mM $MgCl_2$. The bio-5′-AMP solution used in preparing the complexes was made immediately before use by diluting a concentrated stock solution (in water) into the working buffer. Samples were prepared at three loading concentrations and centrifuged at two rotor speeds, 18K and 22K RPM, with a 12-h interval between each speed (*34*). Control experiments were performed to obtain the reduced molecular weight (σ, see below) of the apoBirA monomer at each buffer condition. Protein concentration distributions were determined using the absorption optical system of the instrument. The step size was 0.001 mm, and each data point represented the average of 3 measurements. Scans made in the absence of bio-5′-AMP were collected at 280 nm. In the presence of bio-5′-AMP, in order to avoid any contribution from the absorbance of the adenosine moiety, scans were collected at 295 nm. The solvent density and the protein extinction coefficient at 295 nm were determined as previously described (*24*). In measurements of temperature-dependence the samples and rotor were equilibrated at each working temperature for 2 h prior to starting centrifugation.

Preparation of DNA for Footprinting. The plasmid pBioZ was digested with *Hin*dIII, and the purified, linearized DNA was labeled with α-^{32}P dATP and dGTP using Klenow fragment (*20*, *35*). The labeled DNA was purified over an Elutip column (Scheicher & Schuell), subjected to ethanol precipitation, final digestion with *Pst*I, and phenol/chloroform extraction. Following ethanol precipitation, the labeled restriction fragment was isolated by electrophoresis on a 1% agarose gel, recovered by electroelution (*35*), and finally purified over an Elutip column. Precipitated radiolabeled DNA was resuspended in TE buffer to an approximate final concentration of 8×10^{-3} pmol/μL (20,000 cpm/μL) and stored at 4 °C.

DNaseI Footprint Titrations. DNaseI footprinting was performed as previously described (*16*) according to a modification of the methods outlined by Brenowitz *et al.* (*36*). In experiments designed to measure the temperature-dependence of DNA binding, the reaction buffer contained 10 mM Tris-HCl (pH 7.50 at the working temperature), 200 mM KCl, 2.5 mM $MgCl_2$, 1 mM $CaCl_2$, 100 μg/mL BSA, 2 μg/mL sonicated calf thymus DNA, 50 μM biotin, and 500 μM ATP. For experiments in which the salt-dependence of DNA binding was measured, the reaction buffer was the same as that used for temperature-dependence measurements with the exception that the KCl concentration ranged from 25 to 350 mM and the pH was adjusted at 20 °C. Each 200 μL binding reaction was prepared in reaction buffer and contained 12,000 cpm of radiolabeled DNA at a final concentration of approximately 20 pM and BirA at an appropriate concentration. Reaction mixtures were equilibrated at the appropriate temperature for 1 h, and DNaseI digestion was initiated by the addition of 5 μL of a freshly prepared DNaseI solution in wash buffer (binding buffer without BSA or calf thymus DNA). The amount of DNaseI added to each reaction was empirically set at each experimental condition to ensure less than 50% digestion of the intact DNA (*36*). After 2 min, the digestion was quenched by the addition of 33 μL of 50 mM Na_2EDTA, and the DNA was precipitated by the addition of 700 μL of 0.4 M NH_4-OAc and 50 μg/mL tRNA in absolute ethanol. Following centrifugation, the pellets were washed twice with 500 μL of cold 80% (v/v) absolute ethanol in water and lyophilized. The resulting dried pellets were resuspended in 7 μL of gel loading buffer containing 80% (v/v) deionized formamide, 1 x TBE, 0.02% (w/v) bromophenol blue, and 0.02% (w/v) xylene cyanol, heated for 10 min at 90 °C, and separated on a 10% denaturing acrylamide gel.

Analysis of Sedimentation Equilibrium Data. Sedimentation equilibrium data were analyzed using a version of the NONLIN program (*37*) adapted for analysis of sedimentation equilibrium data (WinNONLIN). Initially, each scan was analyzed to obtain a reduced molecular weight, σ, that is related to the molecular weight of the sedimenting species by the following relationship (*38*):

$$\sigma = \frac{M(1 - \bar{\nu}\rho)\omega^2}{RT} \quad (1)$$

where $\bar{v}$ is the partial specific volume of the macromolecule in mL/g, ρ is the density of the buffer used in g/mL, ω is the angular velocity of the rotor, R is the gas constant, and T is the temperature in kelvins. The data were also globally analyzed using the following model for a monomer−dimer association reaction (*38*):

$$c_t(r) = \delta c + c_m(r_o)e^{\sigma_{mon}((r^2-r_o^2)/2)} + K_a(c_{mon}(r_o))^2\, e^{2\sigma_{mon}((r^2-r_o^2)/2)} \quad (2)$$

where $c_t(r)$ is the total protein concentration at any radial position, r, δc is the baseline offset of the data, $c_m(r_o)$ is the monomer concentration at some reference position, r_o, and K_a is the equilibrium association constant governing assembly of the monomer and dimer. In the analysis the reduced buoyant molecular mass of a dimer was assumed to be twice the value of that for the monomer, which was obtained by subjecting apoBirA to equilibrium sedimentation in the appropriate working buffer. In all data analysis, individual and global analysis of data sets obtained from samples prepared at multiple loading concentrations and run at multiple speeds were performed. The quality of the fits was assessed from the examination of the square root of the variance and the distribution of the residuals.

Quantitation and Analysis of DNaseI Footprint Titrations. The footprinting gels were dried, exposed to storage phosphor screens for ≥40 h, and directly imaged using the Storm phosphorimaging system (GE Healthcare). The optical densities of bands representative of the bioO binding site at each protein concentration were integrated and binding isotherms were generated as described by Brenowitz *et al.* (*36*). All binding data were analyzed by nonlinear least-squares techniques using Graphpad (Prism). The DNA concentration in the binding reaction mixtures permits the assumption that the free holoBirA concentration is equivalent to the total holoBirA concentration. Data were analyzed using the equation

$$\bar{Y} = \frac{K_{DIM}K_{bioO}[P]^2}{1 + K_{DIM}K_{bioO}[P]^2} \quad (3)$$

that relates the occupancy of the biotin operator site, $\bar{Y}$, to the total repressor (holoBirA) monomer concentration, [*P*]. Data were analyzed using two methods. First, the data were analyzed to obtain the product of the equilibrium dimerization constant and the equilibrium constant governing dimer binding to bioO, $K_{DIM}K_{bioO}$. The total free energy of assembly was calculated from the resolved product of the equilibrium constants using the expression $\Delta G°_{TOT} = -RT \ln K_{DIM}K_{bioO}$. Alternatively, K_{bioO}, the equilibrium association constant governing binding of the holoBirA dimer to bioO, was obtained by fixing the equilibrium association constant, K_{DIM}, governing holoBirA dimerization at the value obtained from sedimentation equilibrium performed in the identical buffer conditions. In principle the monomer−dimer equilibrium that the protein undergoes requires solving the quadratic equation that relates $[P]_{free}$ to $[P]_{tot}$ and K_{DIM}. However, comparisons of the resolved values of K_{bioO} obtained with and without explicit consideration of the protein dimerization equilibrium indicated no difference. This comparison was made for the conditions in which the tightest dimerization was measured (50 mM KCl). The Gibbs free energy of dimer binding was calculated using the expression $\Delta G°_{bioO} = -RT \ln K_{bioO}$. The quality of each fit was assessed by the magnitude of the sum of the square of the residuals and the distribution of the residuals.

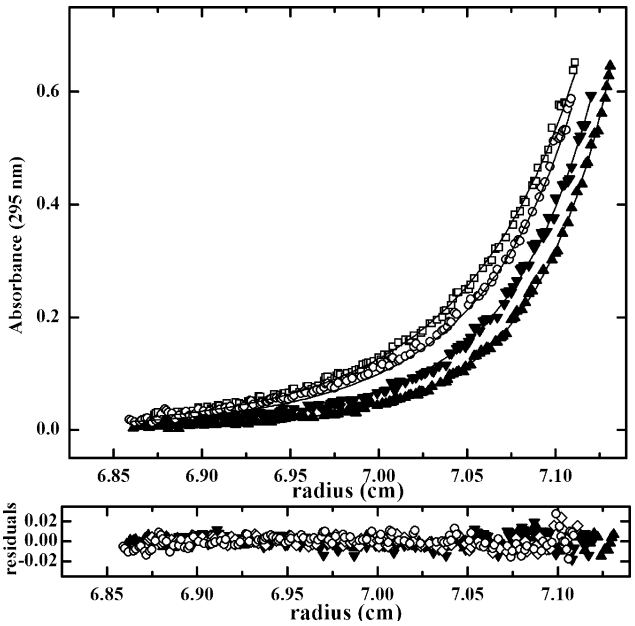

FIGURE 2: Results of sedimentation equilibrium measurements obtained at 5 and 20 °C. The measurements were performed at the indicated temperatures in standard buffer: Loading concentrations were 20 μM (5 °C, open circles; 20 °C, inverted closed triangles) and 55 μM (5 °C, open squares; 20 °C, closed triangles). The rotor speed was 22,000 rpm. The best-fit curves and residuals were obtained from global analysis of data obtained at three loading concentrations and two rotor speeds for the two experimental temperatures. A monomer−dimer model was used in the analysis.

RESULTS

Temperature Dependence of holoBirA Dimerization. HoloBirA (BirA·bio-5′-AMP complex) dimerization measured by sedimentation equilibrium at 20 °C in standard buffer (10 mM Tris-HCl pH 7.50 ± 0.02, 200 mM KCl, 2.5 mM $MgCl_2$) is characterized by an equilibrium dissociation constant between 5 and 10 μM (*23*, *24*). In order to characterize the driving forces for the process the dimerization was measured as a function of temperature from 5 °C to 25 °C. Data obtained at 5 °C and 20 °C shown in Figure 2 indicate that the protein has a lower tendency to self-associate at the lower temperature. The data obtained at 5 °C were first analyzed using a single species model, results of which indicate that, consistent with self-association, the average molecular weight of the protein increases with an increase in the complex concentration loaded in the cell (results not shown). Data were then subjected to global analysis using a monomer−dimer model to obtain the equilibrium dimerization constant. As indicated by the residuals, the fit to this model is excellent. The resolved equilibrium association constant for dimerization obtained at 5 °C is 3.7×10^3 M^{-1}, significantly lower than that obtained at 20 °C (Table 1). Data obtained at all temperatures from 10 °C to 25 °C are also well described by a monomer−dimer model, and inspection of Table 1 reveals that dimerization shows a strong dependence on temperature over the

Table 1: Temperature Dependence of holoBirA Dimerization

T (°C)	K_{DIM} (M^{-1})[a]	$\Delta G°_{DIM}$ (kcal/mol)[b]
5	$4 (\pm 1) \times 10^3$	-4.5 ± 0.1
10	$1.7 (\pm 0.4) \times 10^4$	-5.46 ± 0.01
15	$5 (\pm 1) \times 10^4$	-6.2 ± 0.1
20	$1.4 (\pm 0.1) \times 10^5$	-6.91 ± 0.03
25	$6 (\pm 2) \times 10^5$	-7.9 ± 0.2

[a] Each equilibrium association constant was obtained from global analysis of sedimentation profiles obtained from samples prepared at 3 loading concentrations and centrifuged at 2 rotor speeds. Each reported equilibrium association constant is the average of at least two independent measurements with the 95% confidence interval in parentheses. [b] The Gibbs free energy was calculated using the relationship $-RT \ln K_{DIM}$.

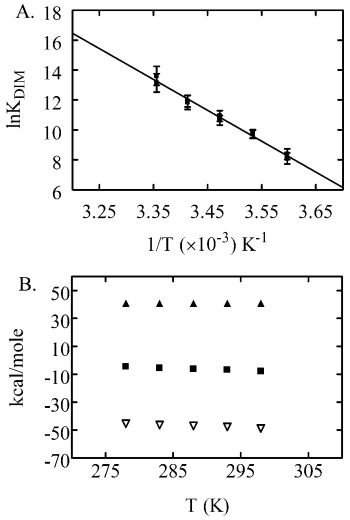

FIGURE 3: (A) Van't Hoff analysis of the temperature dependence of the equilibrium association constant for holoBirA dimerization. The best-fit line represents to results of global analysis of the results of 2−4 independent measurements of the dimerization reaction at each temperature. (B) Thermodynamic profile of dimerization from 5° to 25 °C; $\Delta G°_{DIM}$, closed squares; $\Delta H°_{DIM}$, closed triangles; $-T\Delta S°_{DIM}$, open triangles.

range studied and becomes more favorable with increasing temperature.

In order to obtain the enthalpy of dimerization the temperature dependence of the equilibrium constant for the process was subjected to van't Hoff analysis. The resulting plot, shown in Figure 3A, indicates a linear dependence of the ln K_{DIM} on $1/T$. Linear least-squares analysis of the data yields an enthalpy change for dimerization that is large and positive, $\Delta H_{DIM} = 41 \pm 3$ kcal/mol. Using the equation

$$\Delta G° = \Delta H° - T\Delta S° \quad (4)$$

and the values of the Gibbs free energy for dimerization calculated from the resolved equilibrium association constants obtained at each temperature ($\Delta G° = -RT \ln K_{DIM}$), the entropic contribution to the dimerization process ($-T\Delta S°$) was calculated at each temperature (Figure 3B). At all temperatures employed dimerization is highly entropically favorable and highly enthalpically unfavorable (Table 1). Interestingly, although the dimerization free energy changes by −3.4 kcal/mol as the temperature is increased from 5 to 25 °C, the enthalpy change remains constant. Thus there is no measurable heat capacity change associated with the reaction over this temperature range.

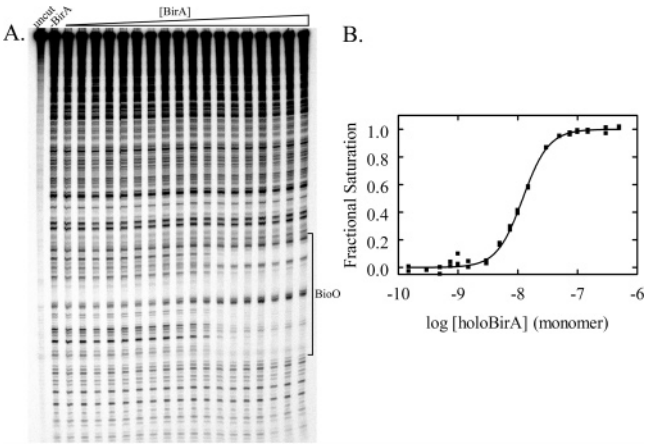

FIGURE 4: (A) Image of the gel obtained for a DNaseI footprint titration performed at 30 °C. The measurement was performed as described in Materials and Methods. (B) Isotherm obtained from quantitation of the data shown in (A). The curve was obtained from nonlinear least-squares analysis of the normalized data using the model shown in eq 3.

Temperature Dependence of DNA Binding. Quantitative DNaseI footprint titrations were used to measure assembly of two holoBirA monomers on bioO. As indicated in Figure 1 assembly of the complex occurs by coupled dimerization and DNA binding. Thus, the isotherm obtained from a footprint titration reflects both steps in the process. Isotherms were analyzed using the following equation:

$$\bar{Y} = \frac{K_{DIM}K_{bioO}[P]^2}{1 + K_{DIM}K_{bioO}[P]^2} \quad (5)$$

in which K_{DIM} is the equilibrium association constant for repressor dimerization, K_{bioO} is the equilibrium association constant for binding of the dimer to bioO, and [P] is the total holoBirA monomer concentration. Analysis of the data can yield information about both the total assembly energetics, $\Delta G°_{TOT}$, and the energetics of holoBirA dimer binding to bioO, $\Delta G°_{bioO}$ (see Figure 1). While in standard buffer at 20 °C the total Gibbs free energy for assembly of two holoBirA monomers on DNA is approximately −21 kcal/mol, the DNA binding free energy is −14 kcal/mol. DNaseI footprint titrations were performed over a range of temperatures in order to determine the driving forces for both the total assembly process and the DNA binding step alone.

An image of a footprint obtained from a titration performed at 30 °C is shown in Figure 4A, and the isotherm obtained from quantitation of the footprint is shown in Figure 4B. Nonlinear least-squares analysis of the data using the model shown in eq 2 was performed to obtain both the product of the equilibrium association constants $K_{DIM}K_{bioO}$ and, using the resolved value of K_{DIM} obtained from sedimentation equilibrium measurements, K_{bioO}. As shown in the figure, the data are well described by the binding model. Resolved parameters shown in Table 2 indicate that while the total free energy of assembly, $\Delta G°_{TOT}$, differs from that measured at 20 °C, the free energy of bioO binding by the dimer, $\Delta G°_{bioO}$ is, within the error of the measurement, the same at the two temperatures. Titrations performed over a temperature range from 5 to 30 °C produced footprints that are qualitatively identical, and analysis of the data yielded the thermodynamic parameters shown in Table 2. The total free

Table 2: Temperature Dependence of Total Assembly and holoBirA Dimer Binding to bioO

T (°C)	$K_{DIM}K_{bioO}$ (M^{-2})[a]	$\Delta G°_{TOT}$ (kcal/mol)	K_{bioO} (M^{-1})[b]	$\Delta G°_{bioO}$ (kcal/mol)
5	$1.5 (\pm 0.5) \times 10^{14}$	-18.0 ± 0.2	$4 (\pm 1) \times 10^{10}$	-13.5 ± 0.2
10	$2 (\pm 1) \times 10^{14}$	-18.5 ± 0.1	$1.3 (\pm 0.3) \times 10^{10}$	-13.1 ± 0.1
15	$4.2 (\pm 0.5) \times 10^{14}$	-19.3 ± 0.1	$9 (\pm 1) \times 10^{9}$	-13.1 ± 0.1
20	$2.3 (\pm 0.4) \times 10^{15}$	-20.6 ± 0.1	$1.6 (\pm 0.3) \times 10^{10}$	-13.7 ± 0.1
25	$2.5 (\pm 0.2) \times 10^{15}$	-21.07 ± 0.04	$3.9 (\pm 0.3) \times 10^{9}$	-13.07 ± 0.04
30	$6 (\pm 2) \times 10^{15}$	-21.8 ± 0.2	$4 (\pm 2) \times 10^{9}$	-13.2 ± 0.2

[a] The DNaseI footprint titration data was directly fit to obtain the product of the equilibrium dimerization constant, K_{DIM}, and the equilibrium constant for holoBirA dimer binding to bioO, K_{bioO}, and the Gibbs free energy term, $\Delta G°_{TOT} = -RT \ln K_{DIM}K_{bioO}$. [b] The equilibrium constant for dimer binding to bioO at each temperature was obtained by subjecting the DNaseI footprint titration data to nonlinear least-squares analysis using the model in eq 3 with K_{DIM} fixed at the value obtained from sedimentation equilibrium measurements. Reported values represent the mean of 2−4 independent measurements performed at each temperature, and the uncertainties reflect the 95% confidence intervals associated with the mean.

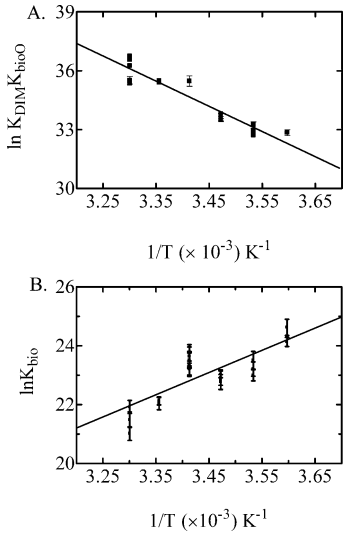

FIGURE 5: Van't Hoff analysis of the temperature dependence of total repression complex assembly (A) and holoBirA dimer binding to bioO (B). Results of 2−4 independent measurements performed at each temperature were subjected to global analysis to obtain the van't Hoff enthalpies.

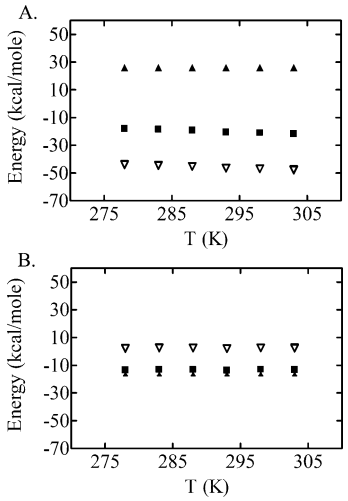

FIGURE 6: Thermodynamic profiles for (A) total repression complex assembly and (B) holoBirA dimer binding to bioO; $\Delta G°_{TOT}$ and $\Delta G°_{bioO}$, closed squares; $\Delta H°_{TOT}$ and $\Delta H°_{bioO}$, closed triangles; $-T\Delta S°_{TOT}$ and $-T\Delta S°_{bioO}$, open triangles.

energy of assembly of the dimer−DNA complexes from the free monomers and DNA, $\Delta G°_{TOT}$, becomes more favorable with increasing temperature and ranges from −18.0 kcal/mol (5 °C) to −21.9 kcal/mol (30 °C). By contrast, the free energy of dimer binding to bioO, $\Delta G°_{bioO}$, changes little in the same temperature range.

The van't Hoff analyses of the DNaseI footprint titration results are shown in Figure 5. Both the total assembly and the bioO binding step were subjected to analysis. Results obtained for the total assembly are shown in Figure 5A, and linear least-squares analysis of the data yields an enthalpy of 26 ± 2 kcal/mol. The van't Hoff analysis of temperature dependence of the DNA binding step is shown in Figure 5B. In contrast to the van't Hoff plot for total assembly, the plot for dimer binding to bioO exhibits a small positive slope, consistent with a comparatively small negative enthalpy change. Linear least-squares analysis of the data yields a value of $\Delta H°_{bioO}$ of −15 ± 2 kcal/mol. The entropic contributions to the total assembly and the dimer binding step were calculated using the appropriate enthalpic contribution for each step and the Gibbs free energies (Figure 6). While entropic contributions ($-T\Delta S°$) to total assembly are large and favorable over the entire temperature range (Figure 6A), those for dimer binding to bioO are small and unfavorable (Figure 6B). Thus, while dimer binding to bioO is an enthalpically driven process, total assembly is overwhelmingly driven by the entropic component of the Gibbs free energy.

HoloBirA Dimerization Is Coupled to Ion Release. In order to investigate the contribution of electrostatic forces to the dimerization process, the linkage between the equilibrium constant for dimerization and salt concentration was measured using sedimentation equilibrium. Measurements were performed in standard buffer (10 mM TrisHCl pH 7.50 ± 0.02 at 20.0 ± 0.1 °C, 2.5 mM $MgCl_2$) prepared at KCl concentrations ranging from 50 to 300 mM. In all cases measurements were performed at three loading concentrations and data were collected at two rotor speeds. Global analysis indicates that the data are well described by a monomer−dimer model over the entire KCl concentration range employed. The plot of ln K_{DIM} vs ln [KCl] shown in Figure 7 indicates, within experimental error, a linear dependence. Linear regression of the data yielded a value for $\delta \ln K_{DIM}/\delta \ln$ [KCl] equal to −1.5 ± 0.1 (Figure 7A). The dimerization process is destabilized by 1.3 kcal/mol as KCl concentration is increased from 50 to 300 mM (Table 3).

Electrostatic Contribution to DNA Binding. DNaseI footprint titrations were used to determine the electrostatic contribution to total assembly of the protein−DNA complex as well as binding of the holoBirA dimer to DNA. Footprints obtained in standard buffer prepared with [KCl] ranging from 25 to 350 mM were qualitatively similar, and even at the lowest KCl concentration no evidence for nonspecific binding

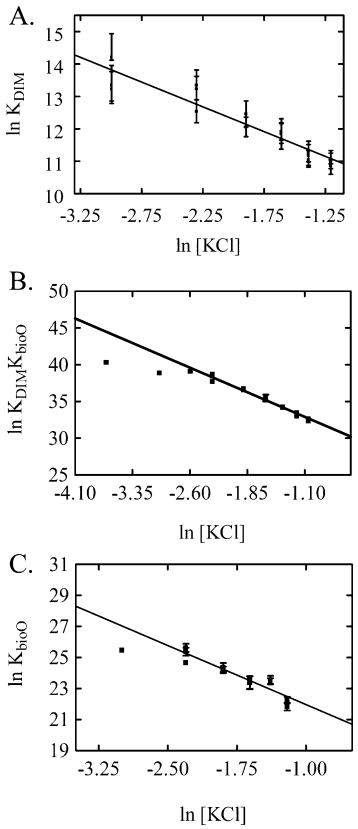

FIGURE 7: Dependence of repression complex assembly on salt concentration. (A) Linkage between holoBirA dimerization and increasing [KCl] measured by sedimentation equilibrium. (B, C) Linkage between total assembly of the repression complex and holobirA dimer binding to bioO on increasing [KCl]. Measurements were performed as described in Materials and Methods, and the lines represent the result of linear least-squares analysis of the data to the relationships described in the Results section. With the exception of the total assembly reaction measured at 25 mM KCl, results from 2−4 independent measurements were included in the analysis.

Table 3: Dependence of holoBirA Dimerization on [KCl]

[KCl] (mM)	K_{DIM} (M^{-1})[a]	$\Delta G°_{DIM}$ (kcal/mol)
50	$7 (\pm 3) \times 10^5$	-7.8 ± 0.3
100	$5 (\pm 1) \times 10^5$	-7.6 ± 0.3
150	$2 (\pm 1) \times 10^5$	-7.2 ± 0.2
200	$1.4 (\pm 0.4) \times 10^5$	-6.9 ± 0.2
250	$4 (\pm 1) \times 10^4$	-6.2 ± 0.2
300	$7 (\pm 2) \times 10^4$	-6.5 ± 0.2

[a] Each equilibrium constant for holoBirA dimerization was obtained from sedimentation equilibrium measurements performed as described in Materials and Methods. The reported values represent the calculated mean of the results of 2−4 independent measurements of the equilibrium association constant for dimerization. The uncertainties are the 95% confidence intervals of the calculated mean.

of the repressor was observed. Data analysis of the isotherms obtained from quantitation of the footprints indicates that the binding is well described by the coupled dimerization and DNA binding model over the entire range of salt concentration.

The total assembly of the $(holoBirA)_2$•bioO complex becomes less favorable with increasing salt concentration with the Gibbs free energy increasing from −23.4 to −18.9 kcal/mol upon increasing the KCl concentration from 25 to 350 mM. The linkage between the total assembly and salt concentration was analyzed by plotting the ln $K_{DIM}K_{bioO}$ versus ln[KCl] (Figure 7B), the results of which reveal a linear dependence at the monovalent salt concentration above 50 mM. This deviation from linearity at the lower salt concentrations may be due to the presence of divalent cations, Ca^{2+} and Mg^{2+}, in the buffer used in footprint titrations, both of which are required for the activity of the cleavage enzyme, DNaseI (*15*, *39*). The slope of the linear dependence observed at monovalent salt concentrations greater than 50 mM can provide an estimate of the net stoichiometry of ion uptake or release upon complex formation. This analysis indicates that approximately 4.5 ± 0.2 ions (cations and/or anions) are released in the assembly of two holoBirA monomers on bioO.

The salt-dependence of holoBirA dimer binding to DNA was deconvoluted from the total assembly by analyzing the footprinting data using the coupled dimerization and DNA binding model with the K_{DIM} fixed at the values obtained from sedimentation equilibrium measurements. Since dimerization at 25 mM KCl was outside of the range measurable by sedimentation equilibrium and was not measured at 350 mM KCl the analysis was performed from 50 mM to 300 mM KCl. A plot of resolved ln K_{bioO} vs ln [KCl] is shown in Figure 7C. In the moderate salt concentrations utilized for these measurements the following equation can be used to analyze the linkage between DNA binding and salt concentration (*15*):

$$\left(\frac{\partial \ln K_{bioO}}{\partial \ln [KCl]}\right)_{T,p,Mg^{2+},Ca^{2+}} = -\Delta n_{K^+} - \Delta n_{Cl^-} \qquad (6)$$

where Δn_{K^+} and Δn_{Cl^-} are the stoichiometries of monovalent cation and anion release or uptake, at constant divalent ion concentration, that are coupled to the DNA binding process. One caveat to analysis of the data presented in this work is that, due to the requirement by DNaseI for the divalent cations, Ca^{2+} and Mg^{2+}, there is some attenuation of the effect of changing monovalent salt concentration on the protein−DNA interaction (*15*, *39*). Indeed the slight curvature in the plot in Figure 7B is consistent with competition from the divalent cations at low monvalent salt concentration. However, as the monovalent cation concentration is increased this effect is minimized. The data from 100 mM and above were fit to a linear equation which yielded a slope, $\delta \ln K_{bio}/\delta \ln [KCl]$, of 2.6 ± 0.2, suggesting net release of 2−3 ions upon binding of the holoBirA dimer to bioO. The sum of the net ion release associated with dimer binding to DNA (2.6 ± 0.2) and that associated with dimerization (1.5 ± 0.1) is, within error, equal to the estimated value of 4.5 ± 0.2 ions released in the total assembly reaction.

DISCUSSION

In this work measurement of assembly of the $(holoBirA)_2$•bioO complex allowed characterization of the driving forces associated not only with the total assembly process but also with the component protein−protein and protein−DNA association reactions. The results indicate that the thermodynamic signature of total assembly is dominated by the dimerization step. Measurements of the dependence of the process on salt concentration indicate that electrostatic effects contribute modestly to both steps in the assembly. The relationship of these results to the structural features of the

Table 4: [KCl] Dependence of Total Repression Complex Assembly and holoBirA Dimer Binding to bioO

[KCl] (mM)	$K_{DIM}K_{bioO}$ (M^{-2})[a]	$\Delta G°_{TOT}$ (kcal/mol)	K_{bioO} (M^{-1})[b]	$\Delta G°_{bioO}$ (kcal/mol)
25	$3 (\pm 1) \times 10^{17}$	-23.4 ± 0.2	nd[c]	nd
50	$7 (\pm 1) \times 10^{16}$	-22.6 ± 0.1	$1.0 (\pm 0.2) \times 10^{11}$	-14.8 ± 0.1
100	$4 (\pm 3) \times 10^{16}$	-22.3 ± 0.3	$9 (\pm 6) \times 10^{10}$	-14.7 ± 0.3
150	$8 (\pm 1) \times 10^{15}$	-21.3 ± 0.1	$3.5 (\pm 0.4) \times 10^{10}$	-14.1 ± 0.1
200	$2.3 (\pm 0.4) \times 10^{15}$	-20.6 ± 0.1	$1.6 (\pm 0.3) \times 10^{10}$	-13.7 ± 0.1
250	$6.9 (\pm 0.4) \times 10^{14}$	-19.88 ± 0.03	$1.6 (\pm 0.1) \times 10^{10}$	-13.68 ± 0.03
300	$3 (\pm 1) \times 10^{14}$	-19.3 ± 0.2	$4 (\pm 1) \times 10^{9}$	-12.8 ± 0.2
350	$1 (\pm 0.3) \times 10^{14}$	-18.9 ± 0.1	nd[c]	nd

[a] The DNaseI footprint titration data was directly fit to obtain the product of the equilibrium dimerization constant, K_{DIM}, and the equilibrium constant for holoBirA dimer binding to bioO, K_{bioO}, and the Gibbs free energy term was calculated using $\Delta G°_{TOT} = -RT \ln K_{DIM}K_{bioO}$. [b] The equilibrium constant for dimer binding to bioO at each temperature was obtained by subjecting the DNaseI footprint titration data to nonlinear least-squares analysis using the model in eq 3 with K_{DIM} fixed at the value obtained from sedimentation equilibrium measurements. [c] Since the dimerization constant was not determined at 25 and 350 mM KCl, the corresponding terms for holoBirA dimer binding to bioO were also not determined. All reported values of $K_{DIM}K_{bioO}$ and K_{bioO} represent the mean of the values obtained from 2−4 independent footprint titrations and uncertainties are the 95% confidence intervals of this mean.

system and the biology of the biotin regulatory system is discussed below.

HoloBirA Dimerization Is Characterized by Large Opposing Enthalpic and Entropic Forces. Measurement of the temperature-dependence of holoBirA dimerization reveals a relatively modest Gibbs free energy, which ranges from −4.5 to −8.6 kcal/mol, for the process over the temperature range studied (5 °C to 25 °C). Van't Hoff analysis of the data indicates a temperature-independent enthalpy of 41 kcal/mol. Thus, in the temperature range employed for these studies the driving force for the process is a large favorable entropy ($-T\Delta S°$). Moreover, the linear dependence of ln K_{DIM} on $1/T$ indicates that, in this same temperature range, dimerization is not accompanied by a heat capacity change. In the repressor dimer structure with BirA bound to the bio-5′-AMP analogue, btnOH-AMP, side-by-side alignment of the central β-sheets of the two monomers results in formation of an extended intermolecular β-sheet. Some fraction of the unfavorable dimerization enthalpy may arise from exchanging the hydrogen bonds of protein groups with solvent for hydrogen bonds with backbone groups on the second monomer. In the context of this interpretation of the unfavorable enthalpy, an explanation for the large favorable entropic term lies in the entropy gain associated with solvent release into the bulk.

The observation that repressor dimerization becomes energetically more favorable with increasing temperature has potential implications for the biology of the *E. coli* biotin regulatory system. Protein−protein interactions are key to the regulation of function in this system. As indicated in the introductory comments, the repressor is also the enzyme that catalyzes biotinylation of the biotin-dependent carboxylase, ACC. While homodimerization is required for holoBirA binding to bioO, the enzymatic function requires that a holoBirA monomer bind to the BCCP subunit of ACC. Moreover, modeling studies (*30*) and the experimentally determined structure of a *Pyrococcus horikoshii* holoBirA·BCCP complex (Bagautdinov, personal communication) indicate that the same surface on holoBirA is utilized for both homo- and heterodimerization. Consequently, holoBirA function reflects competition between mutually exclusive dimerization processes. Results of previous measurements indicate that at 20 °C heterodimerization and homodimerization occur with similar equilibrium constants (*40*). Based on extrapolation of the temperature dependence determined in this work, the equilibrium association constant for holoBirA dimerization is predicted to be 8.1×10^6 M^{-1} (dissociation constant = 0.12 μM) at the physiological temperature of 37 °C. The ability of heterodimerization to compete with homodimerization in the cell will depend on how the holoBirA−apoBCCP interaction varies with temperature.

Contrasting Thermodynamic Signatures of DNA Binding and Total Assembly of the Transcription Repression Complex. Measurement of DNA binding using the footprint titration method allowed determination of the thermodynamic driving forces for total assembly of the $(holoBirA)_2$·bioO repression complex. The energetics of holoBirA dimer binding to the operator were deconvoluted from total assembly energetics using the independently measured Gibbs free energy of dimerization. Discussion of the results will first focus on this DNA binding step.

The Gibbs free energy for dimer binding to bioO changes little as the temperature is increased from 5 to 30 °C. Van't Hoff analysis of the dependence of the equilibrium constant for the process on temperature indicates that it is enthalpically driven and that the enthalpy is constant over the temperature range employed. Thus, in contrast to the dimerization step, binding of the dimer to bioO is enthalpically favored and entropically disfavored (Figure 8). In addition, as observed for the dimerization step, no heat capacity change is associated with the binding process. Many protein−DNA binding reactions have previously been subjected to this type of thermodynamic analysis (*13*), and, in general, they are driven by large opposing enthalpic and entropic forces. However, since enthalpies of binding can range from + 20 to −40 kcal/mol, the favorable driving force can reside in either the enthalpic or the entropic component of the Gibbs free energy. Some correlation has been observed between the degree of distortion of the DNA upon complex formation and the magnitude of the unfavorable enthalpy change associated with the binding process. Solution structural probing of the $(holoBirA)_2$·bioO complex indicates that the DNA is distorted upon protein binding (*32*). Either the distortion is minor and is, therefore, characterized by a small enthalpic penalty or the distortion penalty is compensated by the favorable enthalpy associated with formation of noncovalent bonds in the complex. The source of the modest unfavorable entropy of DNA binding in this system, while

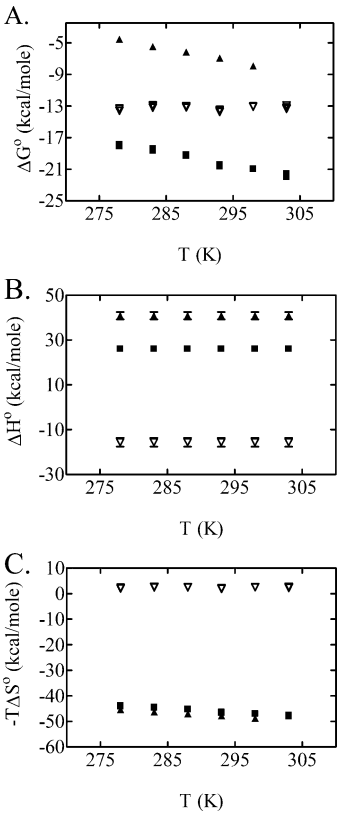

FIGURE 8: Thermodynamics of assembly of the $(holoBirA)_2$·bioO complex from two holoBirA monomers and the free DNA. (A) Gibbs free energy, (B) enthalpy, and (C) entropy for the total assembly (closed squares) and each of the contributing steps including holoBirA dimerization (closed triangles) and holoBirA dimer binding to bioO (open triangles).

not known, is consistent with its modest salt dependence (see below).

The Dimerization Step Dominates the Thermodynamics of Repression Complex Assembly. While the DNA binding step provides a greater fraction of the total free energy to the process, the thermodynamic profile of assembly of the $(holoBirA)_2$·bioO complex from the repressor monomers and free DNA is dominated by the thermodynamic signature for dimerization. The total free energy of assembly ranges from −18 to −22 kcal/mol over the temperature range studied. Dimerization contributes only −4.5 to −8 kcal/mol to the process over the same temperature range (Figure 8). The free energy of dimer binding to bioO changes little over the same temperature interval. While dimerization is characterized by very large opposing enthalpic and entropic contributions to the free energy, DNA binding by the dimer has relatively modest favorable enthalpic and very modest unfavorable entropic driving forces. Analysis of the two convoluted processes reveals that the overall assembly is characterized by a thermodynamic profile similar to that of the dimerization step.

The dominance of the protein−protein interaction in the thermodynamic profile of repression complex assembly indicates the importance of measuring all contributing equilibria in assembly of transcription regulatory complexes. In this system, conclusions based solely on the temperature dependence of the total assembly measured by the DNaseI footprinting technique differ significantly from those based on the combined footprinting and sedimentation equilibrium measurements. Based on the DNaseI footprinting titrations alone one might conclude that holoBirA binding to bioO is characterized by a large unfavorable enthalpy. Results from other systems suggest that one structural interpretation of this unfavorable enthalpy is protein-induced DNA distortion (*13*). However, deconvolution of the DNA binding step from repressor dimerization reveals that the former binding event is enthalpically driven and opposed by a very small entropy ($-T\Delta S°$). Reasonable structural interpretations of this deconvoluted thermodynamic profile differ significantly from that associated with the total assembly reaction.

Electrostatic Contributions to holoBirA Dimerization and DNA Binding Are Modest. The contribution of electrostatic interactions to holoBirA dimerization was measured by sedimentation equilibrium. Analysis of the linkage between the equilibrium constant for the process and salt activity reveals that dimerization becomes weaker with increasing [KCl]. Ion release occurs upon dimer formation, and the linkage analysis reveals that the net number released is 1.5. Application of this simple linkage analysis assumes no influence of the Mg^{2+} in the buffer on the dimerization process. If the ion-linkage is localized to the protein−protein interface, the structure of the BirA·btnOH-AMP complex can be used as a guide for interpreting the electrostatic effect. Inspection of the dimer interface reveals an intermolecular salt bridge between the side chains of D197 and R119 as well as an intramolecular salt bridge between the D197 and K194 side chains. We have previously shown that mutation of either R119 or D197 greatly compromises the holoBirA dimerization (*41*). Formation of this network of ionic interactions upon dimerization may be coupled to the measured ion release.

Both the total assembly reaction and holoBirA dimer binding to bioO exhibit a modest dependence on increasing salt concentration with 4.5 ± 0.2 and 2.5 ± 0.3 ions released, respectively, in the two processes. Since the DNaseI footprint titrations were performed in the presence of competing divalent cations, Ca^{2+} and Mg^{2+}, these numbers are likely lower than would be measured in buffers containing only the monovalent salt. However, attempts to use DNA binding techniques other than DNaseI footprinting on the holoBirA−bioO binding system have been unsuccessful. The curvature in the plots of the dependence of both total assembly and the DNA binding step on ln [KCl] is consistent with this competition from the divalent cations. This curvature is also consistent with release of anions by holoBirA upon binding to bioO. However, even in the context of the caveats associated with the analysis, the net ion release of 2.5 ± 0.3 upon binding of the holoBirA dimer to bioO is low. Given structural information available for the complex, a large number of cations are anticipated to be released upon dimer binding. The operator sequence is forty base-pairs, and results of hydroxyl radical protection studies indicate protection of approximately 20 phosphodiester backbone groups from cleavage in the complex (Figure 1B). The low apparent stoichiometry of ion release upon binding of the holoBirA dimer to bioO reflects either the retention of ions on the DNA in the complex or the linkage of compensating ion uptake by the protein to DNA binding. More extensive studies using mixed-composition salts would be required to elucidate the basis of the apparently modest electrostatic contribution to holoBirA dimer binding to bioO.

ACKNOWLEDGMENT

The authors would like to thank Drs. Aditi Gupta and Patrick Brown for performing some of the measurements of holoBirA dimerization reported in this paper.

REFERENCES

1. Choi, K. Y., and Zalkin, H. (1992) Structural characterization and corepressor binding of the *Escherichia coli* purine repressor, *J. Bacteriol. 174*, 6207−6214.
2. Schumacher, M. A., Choi, K. Y., Zalkin, H., and Brennan, R. G. (1994) Crystal structure of LacI member, PurR, bound to DNA: minor groove binding by alpha helices, *Science 266*, 763−770.
3. Schevitz, R. W., Otwinowski, Z., Joachimiak, A., Lawson, C. L., and Sigler, P. B. (1985) The three-dimensional structure of trp repressor, *Nature 317*, 782−786.
4. Carey, J. (1988) Gel retardation at low pH resolves trp repressor-DNA complexes for quantitative study, *Proc. Natl. Acad. Sci. U.S.A. 85*, 975−979.
5. Otwinowski, Z., Schevitz, R. W., Zhang, R. G., Lawson, C. L., Joachimiak, A., Marmorstein, R. Q., Luisi, B. F., and Sigler, P. B. (1988) Crystal structure of trp repressor/operator complex at atomic resolution, *Nature 335*, 321−329.
6. Riggs, A. D., and Bourgeois, S. (1968) On the assay, isolation and characterization of the lac repressor, *J. Mol. Biol. 34*, 361−364.
7. Riggs, A. D., Suzuki, H., and Bourgeois, S. (1970) Lac repressor-operator interaction. I. Equilibrium studies, *J. Mol. Biol. 48*, 67−83.
8. Sauer, R. T. (1979) Ph.D. Dissertation, Harvard University, Cambridge, MA.
9. Darling, P. J., Holt, J. M., and Ackers, G. K. (2000) Coupled energetics of lambda cro repressor self-assembly and site-specific DNA operator binding II: cooperative interactions of cro dimers, *J. Mol. Biol. 302*, 625−638.
10. Kewley, R. J., Whitelaw, M. L., and Chapman-Smith, A. (2004) The mammalian basic helix-loop-helix/PAS family of transcriptional regulators, *Int. J. Biochem.* Cell Biol *36*, 189−204.
11. Beckett, D., Koblan, K. S., and Ackers, G. K. (1991) Quantitative study of protein association at picomolar concentrations: the lambda phage cl repressor, *Anal. Biochem. 196*, 69−75.
12. Koblan, K. S., and Ackers, G. K. (1992) Site-specific enthalpic regulation of DNA transcription at bacteriophage lambda OR, *Biochemistry 31*, 57−65.
13. Jen-Jacobson, L., Engler, L. E., and Jacobson, L. A. (2000) Structural and thermodynamic strategies for site-specific DNA binding proteins, *Structure 8*, 1015−1023.
14. Spolar, R. S., and Record, M. T., Jr. (1994) Coupling of local folding to site-specific binding of proteins to DNA, *Science 263*, 777−784.
15. Record, M. T., Jr., Ha, J. H., and Fisher, M. A. (1991) Analysis of equilibrium and kinetic measurements to determine thermodynamic origins of stability and specificity and mechanism of formation of site-specific complexes between proteins and helical DNA, *Methods Enzymol. 208*, 291−343.
16. Koblan, K. S., and Ackers, G. K. (1991) Energetics of subunit dimerization in bacteriophage lambda cI repressor: linkage to protons, temperature, and KCl, *Biochemistry 30*, 7817−7821.
17. Koblan, K. S., and Ackers, G. K. (1991) Cooperative protein-DNA interactions: effects of KCl on lambda cI binding to OR, *Biochemistry 30*, 7822−7827.
18. Barker, D. F., and Campbell, A. M. (1981) The birA gene of *Escherichia coli* encodes a biotin holoenzyme synthetase, *J. Mol. Biol 146*, 451−467.
19. Barker, D. F., and Campbell, A. M. (1981) Genetic and biochemical characterization of the birA gene and its product: evidence for a direct role of biotin holoenzyme synthetase in repression of the biotin operon in Escherichia coli, *J. Mol. Biol. 146*, 469−492.
20. Abbott, J., and Beckett, D. (1993) Cooperative binding of the *Escherichia coli* repressor of biotin biosynthesis to the biotin operator sequence, *Biochemistry 32*, 9649−9656.
21. Prakash, O., and Eisenberg, M. A. (1979) Biotinyl 5′- adenylate: corepressor role n the regulation of the biotin genes of *Escherichia coli* K-12., *Proc. Natl. Acad. Sci. U.S.A 76*, 5592−5595.
22. Lane, M. D., Rominger, K. L., Young, D. L., and Lynen, F. (1964) The enzymatic synthesis of holotranscarboxylase from apotranscarboxylase and (+)-biotin, *J. Biol. Chem 239*, 2865−2871.
23. Eisenstein, E., and Beckett, D. (1999) Dimerization of the *Escherichia coli* biotin repressor: corepressor function in protein assembly, *Biochemistry 38*, 13077−13084.
24. Streaker, E. D., Gupta, A., and Beckett, D. (2002) The biotin repressor: thermodynamic coupling of corepressor binding, protein assembly, and sequence-specific DNA binding, *Biochemistry 41*, 14263−14271.
25. Streaker, E. D., and Beckett, D. (2003) Coupling of protein assembly and DNA binding: biotin repressor dimerization precedes biotin operator binding, *J. Mol. Biol. 325*, 937−948.
26. Wilson, K. P., Shewchuk, L. M., Brennan, R. G., Otsuka, A. J., and Matthews, B. W. (1992) *Escherichia coli* biotin holoenzyme synthetase/bio repressor crystal structure delineates the biotin- and DNA-binding domains, *Proc. Natl. Acad. Sci. U.S.A. 89*, 9257−9261.
27. Weaver, L. H., Kwon, K., Beckett, D., and Matthews, B. W. (2001) Corepressor-induced organization and assembly of the biotin repressor: a model for allosteric activation of a transcriptional regulator, *Proc. Natl. Acad. Sci. U.S.A. 98*, 6045−6050.
28. Wood, Z. A., Weaver, L. H., Brown, P. H., Beckett, D., and Matthews, B. W. (2006) Co-repressor induced order and biotin repressor dimerization: a case for divergent followed by convergent evolution, *J. Mol. Biol. 357*, 509−523.
29. Russell, R. B., and Barton, G. J. (1993) An SH2-SH3 domain hybrid, *Nature 364*, 765.
30. Weaver, L. H., Kwon, K., Beckett, D., and Matthews, B. W. (2001) Competing protein:protein interactions are proposed to control the biological switch of the *E. coli* biotin repressor, *Protein Sci. 10*, 2618−2622.
31. Brown, P. H., Cronan, J. E., Grotli, M., and Beckett, D. (2004) The biotin repressor: modulation of allostery by corepressor analogs, *J. Mol. Biol. 337*, 857−869.
32. Streaker, E. D., and Beckett, D. (1998) A map of the biotin repressor-biotin operator interface: binding of a winged helix-turn-helix protein dimer to a forty base-pair site, *J. Mol. Biol. 278*, 787−800.
33. Streaker, E. D., and Beckett, D. (1998) Coupling of site-specific DNA binding to protein dimerization in assembly of the biotin repressor-biotin operator complex, *Biochemistry 37*, 3210−3219.
34. Roark, D. E. (1976) Sedimentation equilibrium techniques: multiple speed analyses and an overspeed procedure, *Biophys. Chem. 5*, 185−196.
35. Maniatis, T., Fritsch, E.F., & ZSambrook, J. (1982) *Molecular Cloning, A Laboratory Manual*, Cold Spring Harbor, Cold Spring Harbor, NY.
36. Brenowitz, M., Senear, D. F., Shea, M. A., and Ackers, G. K. (1986) Quantitative DNase footprint titration: a method for studying protein-DNA interactions, *Methods Enzymol. 130*, 132−181.
37. Johnson, M. L., Correia, J. J., Yphantis, D. A., and Halvorson, H. R. (1981) Analysis of data from the analytical ultracentrifuge by nonlinear least-squares techniques, *Biophys. J. 36*, 575−588.
38. Laue, T. M. (1995) Sedimentation equilibrium as thermodynamic tool, *Methods Enzymol. 259*, 427−452.
39. Record, M. T., Jr., deHaseth, P. L., and Lohman, T. M. (1977) Interpretation of monovalent and divalent cation effects on the lac repressor-operator interaction, *Biochemistry 16*, 4791−4796.
40. Streaker, E. D., and Beckett, D. (2006) The biotin regulatory system: kinetic control of a transcriptional switch, *Biochemistry 45*, 6417−6425.
41. Kwon, K., Streaker, E. D., Ruparelia, S., and Beckett, D. (2000) Multiple disordered loops function in corepressor-induced dimerization of the biotin repressor, *J. Mol. Biol. 304*, 821−833.
42. Koradi, R., Billeter, M., and Wuthrich, K. (1996) MOLMOL: a program for display and analysis of macromolecular structures, *J. Mol. Graphics 14, 51−55*, 29−32.

BI7013097